Review of Scientific Instruments

RESEARCH ARTICLE | SEPTEMBER 30 2024

Long-term stability of squeezed light in a fiber-based system using automated alignment

Tomohiro Nakamura ; Takefumi Nomura; Mamoru Endo ; Atsushi Sakaguchi ; He Ruofan; Takahiro Kashiwazaki ; Takeshi Umeki; Kan Takase ; Warit Asavanant ; Jun-ichi Yoshikawa; Akira Furusawa

Rev. Sci. Instrum. 95, 093004 (2024)
https://doi.org/10.1063/5.0203988
CHORUS

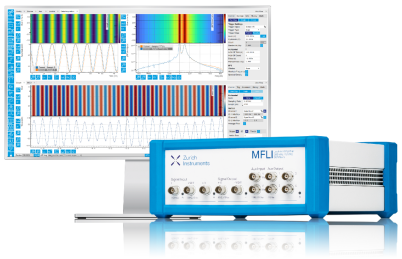

AIP Publishing

Review of Scientific Instruments ARTICLE pubs.aip.org/aip/rsi

Long-term stability of squeezed light in a fiber-based system using automated alignment

Cite as: Rev. Sci. Instrum. 95, 093004 (2024); doi: 10.1063/5.0203988
Submitted: 18 February 2024 • Accepted: 3 September 2024 •
Published Online: 30 September 2024

Tomohiro Nakamura,[1,a)] Takefumi Nomura,[1] Mamoru Endo,[1,2] Atsushi Sakaguchi,[2] He Ruofan,[1] Takahiro Kashiwazaki,[3] Takeshi Umeki,[3] Kan Takase,[1,2] Warit Asavanant,[1,2] Jun-ichi Yoshikawa,[2] and Akira Furusawa[1,2,b)]

AFFILIATIONS

[1] Department of Applied Physics, School of Engineering, The University of Tokyo, 7-3-1 Hongo, Bunkyo-ku, Tokyo 113-8656, Japan
[2] Optical Quantum Computing Research Team, RIKEN Center for Quantum Computing, 2-1, Hirosawa, Wako 351-0198, Saitama, Japan
[3] NTT Device Technology Labs, NTT Corporation, 3-1, Morinosato Wakamiya, Atsugi 243-0198, Kanagawa, Japan

[a)] **Electronic mail:** nakamura@alice.t.u-tokyo.ac.jp
[b)] **Author to whom correspondence should be addressed:** akiraf@ap.t.u-tokyo.ac.jp

ABSTRACT

Providing a cloud service for optical quantum computing requires stabilizing the optical system for extended periods. It is advantageous to construct a fiber-based system, which does not require spatial alignment. However, fiber-based systems are instead subject to fiber-specific instabilities. For instance, there are phase drifts due to ambient temperature changes and external disturbances and polarization fluctuations due to the finite polarization extinction ratio of fiber components. Here, we report the success of measuring squeezed light with a fiber system for 24 h. To do this, we introduce stabilization mechanics to suppress fluctuations in the fiber system and an integrated controller to automatically align the entire system. The squeezed light at a wavelength of 1545.3 nm is measured every 2 min, where automated alignments are inserted every 30 min. The squeezing levels with an average of −4.42 dB are recorded with an extremely small standard deviation of 0.08 dB over 24 h. With the technologies developed here, we can build complicated optical setups with the fiber-based system and operate them automatically for extended periods, which is promising for cloud service of quantum computation.

I. INTRODUCTION

To accelerate research and development of quantum computation, it is desired to open prototypes and allow researchers to access them. Google and IONQ have developed high-fidelity 11-qubit ion-trap quantum computing accessible via Google Cloud.[1] IBM has released a superconducting 127-qubit quantum processor, "Eagle," in 2021 on the IBM Cloud.[2] Xanadu has conceived and built "Borealis," a free-space-based quantum processor that can perform Gaussian boson sampling,[3] and made it available on their cloud platform. Since the "Borealis" is a free-space system except for some parts of the system, pointing of the optical beam drifts, which is recovered by frequent manual alignments. If the system is constructed with a fiber system instead of a free-space system, the frequent alignments are removed. Thus, the fiber system is advantageous when constructing a quantum computer operating for a long time.

In particular, we are aiming to build a fiber-based optical quantum computer that operates on continuous variables of light. Quantum computation based on continuous variables is gaining attention. Recently, large-scale entanglements using time-domain multiplexing and frequency-domain multiplexing have been demonstrated.[4–14] In time-domain multiplexing, large entanglement is generated by sending squeezed light to interferometers with asymmetric lengths of arms.

However, if the optical system is constructed with fiber, fiber-specific problems arise. Phase drifts and polarization fluctuations are caused by ambient temperature changes.[15–17] For phase drifts, an

optical delay of 10 m in free-space systems causes typically a few wavelengths of phase drift in 1 min, while that in the fiber system, if no measures are taken, induces several hundred wavelengths of phase drift in 1 min. For polarization drifts, even if polarization-maintaining fibers are used, the polarization extinction ratio (PER) of fiber components is finite, and thus, concatenating these devices leads to polarization instability. Typically, polarization drift is several degrees on the Poincaré sphere over 1 h. Furthermore, power fluctuations are induced by the polarization fluctuations when combined with polarization-dependent components. In addition, the coupling ratio of the fiber beam splitter is slightly dependent on the polarization and temperature. Since the squeezed light is degraded by optical loss, all fiber components through which the squeezed light passes should have low optical loss.

Here, we solve the above issues by introducing stabilization devices and successfully measure squeezed light stably for 24 h. For phase drifts, we cover the entire system with a windshield to passively suppress large phase drifts and then introduce the fiber stretchers to actively suppress the phase drifts with feed-back controls. For polarization fluctuations, various technologies for polarization optimization are discussed in papers.[18–26] In this experiment, active polarization controllers are introduced together with polarizers. In order to generate the error signal for the polarization control, a polarization modulation method is employed. For power fluctuations, a power stabilization mechanism is introduced. For a fiber beam splitter whose coupling ratio variation is critical, we control the temperature of the beam splitter and stabilize the coupling ratio without introducing significant optical loss. Automated alignment of the entire system is achieved by connecting the various stabilization mechanisms via a network and integrating their control program. Using the above system, we measure the squeezed light in 1545.3 nm generated by the optical parametric amplifier (OPA) with a periodically poled lithium niobate (PPLN) waveguide[27,28] at 2-min intervals with automated alignment every 30 min. Squeezing levels with an average of −4.42 dB and the standard deviation of 0.08 dB are successfully measured over 24 h. In this demonstration, the optical loss of squeezed light is avoided by placing the controllers in the paths where the squeezed light does not pass, except for the coupling ratio stabilization. On the other hand, in the case of a more complex interferometer built for optical quantum computers, there are situations where the polarization and the phase of squeezed light need to be controlled with low optical loss. In that case, the method proposed in Ref. 29 can be available.

There are previous studies that demonstrate quantum optics experiments with fibers. In Ref. 30, with a fiber packaged OPA, squeezed light is measured in fiber-based systems. In Ref. 12, squeezed light from a free-space optical parametric oscillator is injected into fiber interferometers to generate two-dimensional cluster states. However, in the above two demonstrations, the polarization of light and the coupling ratio of fiber beam splitters are controlled manually or uncontrolled. To realize long-time stability, alignment needs to be automated. In Refs. 31 and 32, long-time squeezed light measurements have been reported for free-space systems. These previous experiments are working well because the configurations of the optical setup are relatively simple. For more complex systems realizing optical quantum computers, fiber systems are advantageous, as explained above, and thus, our techniques introduced in this work can be applicable to such complex systems.

This paper is structured as follows: We explain squeezed light in Sec. II. We discuss why various stabilizations are needed in the experimental setup in Sec. III. We illustrate an overview of the experimental system in Sec. IV. We explain the stabilization of optical power in Sec. V, phase lock in Sec. VI, polarization optimization in Sec. VII, and the coupling ratio stabilization of the fiber beam splitter in Sec. VIII. We show the results of the 24-h squeezed light measurement in Sec. IX. Section X is the conclusion.

II. SQUEEZED LIGHT AND MEASUREMENT

The quadrature phase amplitudes $\hat{x}$ and $\hat{p}$ of the single-mode quantized field of light have uncertainty $\Delta(\hat{x})\Delta(\hat{p}) \geq \hbar/2$, where $\hbar$ is the reduced Planck constant. The vacuum state is a minimum uncertainty state with $\Delta(\hat{x}) = \Delta(\hat{p}) = \sqrt{\hbar/2}$. A squeezed state has a quadrature phase amplitude where the fluctuation is smaller than that for a vacuum state.[33] For example, an x-squeezed state is squeezed as $\Delta(\hat{x}) < \sqrt{\hbar/2}$ and instead anti-squeezed as $\Delta(\hat{p}) > \sqrt{\hbar/2}$ to satisfy the uncertainty principle. Fault tolerant quantum computation can be achieved by using high-level squeezed states.[34–36] An arbitrary quadrature phase amplitude $\hat{x}\cos\theta + \hat{p}\sin\theta$ can be measured by setting the phase of the local oscillator (LO) light to θ in an optical homodyne detection. A vacuum state has a quadrature distribution insensitive to θ, while a squeezed state has that sensitive to θ. Figure 1 (right) shows a typical quadrature distribution of an x-squeezed state, where the quadrature has the minimum variance at $\theta = 0, \pi$, and the maximum variance at $\theta = \pi/2, 3\pi/2$.

Figure 1 shows a simplified experimental setup for generating and measuring squeezed light. Here, the angular frequency of fundamental light is ω. By injecting pump light with the angular frequency of 2ω to a second-order nonlinear material, squeezed light is generated by parametric downconversion. In our demonstration here, squeezed light is generated by a PPLN waveguide OPA. The probe light with an angular frequency ω is fed to the OPA as a reference for the phase lock. In our experiment, the angular frequency is shifted from ω to form the beat signal. In homodyne detection, squeezed light is combined with LO light at a 50:50 beam splitter and then is detected with two photodiodes in a homodyne detector, where the difference of the photocurrents shows the quadrature values. The squeezing and antisqueezing levels are obtained by comparing the variances with those of the vacuum state. The quadrature phase amplitude of the vacuum state is obtained by blocking the squeezed light and feeding only the LO light into the homodyne detector. Since the energy of a single photon corresponds to about 12 000 K in the telecommunication wavelength, thermal excitation in the single-mode quantized field of light is negligible at room temperature, and the vacuum state can be measured with this method.

It is necessary to lock the phase of the LO light depending on the measurement phase. For phase lock, coherent light of the fundamental wave is input to the OPA, and this light is referred to as the probe light. Since the probe light undergoes phase-sensitive amplification, which is in phase with the generated squeezed light, the relative phase between the probe light and the squeezed light can be locked. In homodyne detection, the interference signal between the probe light and the LO light is locked, by which the relative phase between the squeezed light and the LO light is locked.

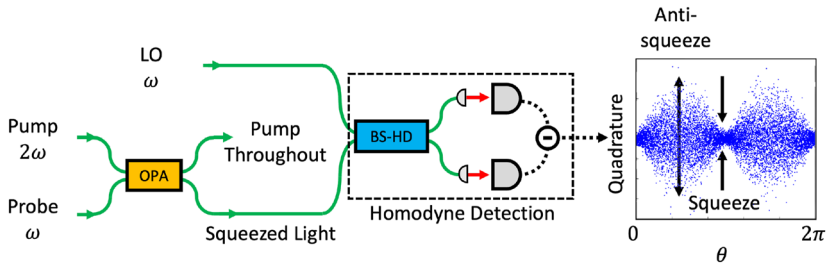

FIG. 1. Fundamental setup for squeezed light measurement. Squeezed light is generated by OPA. The squeezed light is detected by homodyne detection, which measures an arbitrary light quadrature depending on the measurement basis θ. BS: beam splitter, OPA: optical parametric amplifier, HD-BS: beam splitter for homodyne detection, green line: PM fiber, and dotted line: electric wire.

III. NECESSITY FOR STABILIZATION MECHANICS

Although we build the experimental setup for the squeezed light measurement, the stabilization mechanics that are implemented in this system are easily extended to the more complicated system.

In optical quantum computation, interference of squeezed light generates complicated entanglement structures. The polarizations must be matched, and the relative phases must be locked to a specific direction at the interference points. If polarization and phase are not in the proper state, the quality of the entanglement is degraded. Even if the fiber components are made of polarization-maintaining fibers, connections between multiple fiber components shift the polarization state of the light from the polarization-maintaining axis. Birefringence variation caused by external disturbances fluctuates the polarization of light, which is shifted from the polarization-maintaining axis. The polarization fluctuations also cause power fluctuations as the light passes through the polarization-dependent element. For example, fluctuations in LO power cause changes in the shot noise level in homodyne detections, which undermines the reliability of the experiment. Furthermore, changes in ambient temperature cause the fiber to expand and contract, which changes the optical path length, resulting in phase drift.[37] In addition, a fiber beam splitter can be realized with a directional coupler, but its coupling ratio must be stable at an appropriate value.

In the squeezed light measurement experiments of this study shown in Fig. 1, the issues of polarization fluctuation, power fluctuation, phase drift, and coupling ratio fluctuation of the beam splitter appear as follows: and stabilization mechanics are installed. Regarding polarization, if the polarizations of the squeezed light and the LO light are misaligned, the squeezing level is degraded. Squeezed light is generated by OPA, but the polarization of the squeezed light is parallel to the crystal axis of the PPLN waveguide. For the polarization alignment, the probe light is input to the path of the squeezed light. The polarization of the probe light is adjusted to match the polarization of the squeezed light, and then the polarization of the LO light is adjusted to match the polarization of the probe light. Polarization controls are implemented with devices that change polarization by applying pressure to the fiber and causing birefringence. In the case of the LO light, power fluctuations change the shot noise level of the homodyne detection. In the case of the probe light, they change the amplitude of the error signals of the various locks, resulting in a misalignment of the locking points. Therefore, it is necessary to stabilize the power of the LO and probe light, and fiber pigtailed variable attenuators are used. As for the phase, if the phase lock is not able to cancel the phase drift, an anti-squeeze component will be mixed when measuring the squeezing level, resulting in the reduction of squeezing level. In these experiments, fiber stretchers are inserted for the phase lock between the pump light and the probe light and for that between the probe light and the LO light. The coupling ratio of the fiber beam splitter used in this study for homodyne detection has severe hysteresis when the knob is rotated, making it difficult to adjust it manually. Furthermore, the polarization of the input light also changes the coupling ratio. Therefore, the coupling ratio is controlled by temperature.

IV. OUTLINE OF THE EXPERIMENTAL SYSTEM

In this study, squeezed light is measured over 24 h with the experimental system shown in Fig. 2. In order to ensure stable measurements, light power stabilization, phase lock, polarization optimization, and coupling ratio lock of the beam splitter are performed, which are described in the following sections. In this section, we describe the entire setup of the experimental system.

The laser source consists of multiple devices. The seed laser is Koheras ADJUSTIK X15 (NKT Photonics), whose wavelength and power are 1545.3 nm and 15 mW, respectively. The preamplifier, which reduces relative power noise by feedback, is Koheras BOOSTIK Linecard (NKT Photonics), whose output power of 80 mW is then attenuated to 20 mW. The main amplifier is Koheras BOOSTIK (NKT Photonics), whose output power is 8 W. The second harmonic generator (SHG) is Koheras HARMONIK (NKT Photonics), which converts some part of 1545.3 nm light to 772.7 nm light. After the SHG, the 1545.3 nm light and the 772.7 nm light are emitted to free space, which are then coupled to fibers. The 1545.3 nm light is used as the probe and LO light and the 772.7 nm light as the pump light. Before the fiber coupling, motor-driven optical shutters are inserted for all light paths to block the light, which is utilized in the sequence of control explained later. Shutters are composed of the motor MS18 (Miuzei) and black aluminum foil.

Fiber components for the probe, the LO, and the pump light are as follows: For the probe path, two acousto-optic modulators (AOMs) SGTF200-1550-1P (Chongqing Smart Science and Technology Development) are inserted. Then, for the probe and the LO

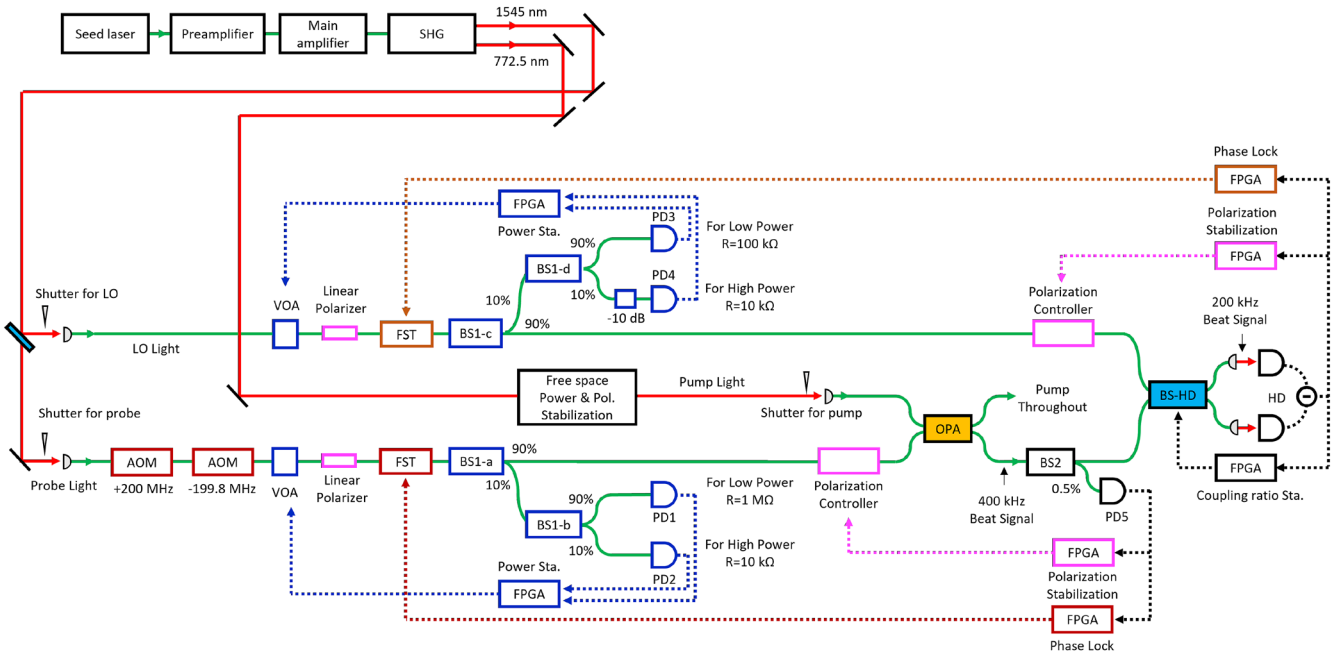

FIG. 2. Experimental system of this study. Blue objects are for light power stabilization, pink objects are for polarization optimization, and brown objects are for phase lock. AOM: acousto optic modulator, VOA: variable optical attenuator, FST: fiber stretcher, and BS: beam splitter, HD-BS: beam splitter for homodyne detection, OPA: optical parametric amplifier, FPGA: field programmable gate array, PD: photo detector, HD: homodyne detector, green line: PM fiber, and dotted line: electric wire.

light paths, a fiber-based variable optical attenuator for power stabilization, a fiber stretcher for phase control, and a polarization controller are connected. In the pump light path, the light power is stabilized by a motorized waveplate and polarizing beam splitter in free space. The probe light and the pump light are input to the OPA, which is a PPLN waveguide and packaged with fiber input and output. The PPLN waveguide inside the OPA is quasi-phase-matched with type 0.[27,28] Only the component parallel to the crystal axis of the input pump light contributes to the generation of squeezed light at the PPLN waveguide. This means that polarization fluctuations of the pump light do not cause polarization fluctuations of the squeezed light. Therefore, for the pump light, only the power stabilization is sufficient, which is performed by a free-space motorized waveplate and a polarizing beam splitter. In the demonstration in Sec. IX, the power of the pump light is set to be 300 mW.

In homodyne detection, the probe light interferes with the LO light at a fiber beam splitter with a coupling ratio of 50:50 and is sent to the homodyne detector. Since the utilized photodiodes are for the free-space light, the light is output to free space by a collimator and focused on the photodiode by a concave mirror with a 100 mm radius of curvature to minimize optical losses. For all-fiber implementation, the photodiodes can be fiber pigtailed in the future. The photodiodes of the homodyne detector are high quantum efficiency InGaAs-PD at 1550 nm (Laser Components) with a quantum efficiency of 96%, which is measured by us. The difference of photocurrents is converted to a voltage signal by a transimpedance amplifier, which is composed of OPA847 (Texas Instruments) and 3 kΩ resistance. The signal from the homodyne detector is used for two purposes. The first is to generate an error signal for the phase lock, the polarization optimization, and the coupling ratio lock of the 50:50 beam splitter. The second is to measure the squeezing level. The signal for the squeezing level measurement is high-pass filtered with a cutoff frequency of 15 MHz, which is selected to cut the beat signal with a frequency of 200 kHz. Then it is amplified by a factor of 15.

Because squeezed light is degraded by optical loss, optical components through which the squeezed light passes should have low optical loss. The fiber beam splitters BS2 and BS-HD are 954P (evanescent optics), which have a loss of less than 0.1 dB. The fiber components are made of polarization maintaining fibers except for the polarization controller.

The power stabilization, the phase lock, the polarization optimization, and the coupling ratio stabilization of the beam splitter need signal processing circuits for feedback control. To implement these, a number of field-programmable gate arrays (FPGAs), STEMlab 125-14 RedPitaya, are utilized. The clock rate is 125 MHz, and the resolution of the inputs and outputs is 14 bits. Infinite response filters and PID feedback are implemented to generate feedback signals for controls.

To realize the automated alignment of the entire system, we need to monitor the status of each experimental instrument and adjust control parameters. Every control device is connected to the single computer by Ethernet cables, or USB cables and we establish the socket communication. Each RedPitaya has server programs, and the computer has client programs. The RedPitaya has an oscilloscope and returns the obtained waveforms to the computer. We

optimize parameters, for example, the cutoff frequency of filters and PID parameters for the feedback control, and send them to each device.

Multiple modulation and demodulation signals are required for phase lock and polarization optimization, which are synchronously generated by a direct digital synthesizer (AD9959, Analog Devices).

V. LIGHT POWER STABILIZATION

In Fig. 2, components that serve for power stabilization are colored blue. To monitor the power fluctuation, some part of the light is picked up and fed back to the variable optical attenuator (NEW MMVOA-1-1550-P-8/125-SCSC-1-0.5, OZ Optics). To pick the light up, beam splitters BS1-a and BS1-c (PMFC-1x2-1550-10/90-B-900-5-1-SC-P25, Opneti) with a coupling ratio of 90:10 are used. To realize automated alignment, the light power needs to be stabilized at different orders of magnitude during alignment and measurement sequence. The target powers of the probe light are 1 μW for the OPA alignment, 100 μW for homodyne alignment, and 100 nW for squeezed light measurement. The target powers of the LO light are 100 μW for alignment and 16 mW for measurement. For the low power, it is necessary to largely amplify weak light, and for the high power, it is necessary to reduce the amount of light to avoid the saturation of the PD. Therefore, the picked-up light is further divided by a 90:10 beam splitter BS1-b, BS1-d, whose model number is the same as that of BS1-a and BS1-c. Then, the divided light goes to the two photo detectors (PDs), one for the high power and one for the low power. PD1, PD2, PD3, and PD4 contain a photodiode G8195-11 (Hamamatsu Photonics) and a transimpedance amplifier, where the transimpedance is 1 MΩ, 10, 100, and 10 kΩ, respectively. Before PD4, a 10 dB attenuator is inserted. Because the finite PER of the fiber components can cause polarization change, the PER of BS1-a, b, c, and d is ordered to be better than 25 dB. For the PID lock by FPGA, the integration term is activated. Without the power stabilization, the optical power drift was 15% at most, but with the power stabilization on, the standard deviation of the power fluctuation was 0.1%.

VI. PHASE LOCK

In Fig. 2, components that serve for phase locks are colored brown. There are two phase lock points: the parametric amplification of the OPA (the phase between the probe light and the pump light) and the homodyne detection (the phase between the probe light and the LO light). The probe light is frequency-shifted by the AOMs before the OPA. The frequency is up-shifted by 200.0 MHz at the first AOM and then down-shifted by 199.8 MHz at the second AOM, resulting in a total frequency shift of 200 kHz. At the OPA, the probe light is parametrically amplified depending on the phase between the probe light and the pump light. The parametric amplification generates −200 kHz detuned light from the 200 kHz detuned probe light, thus resulting in a 400 kHz beat signal. The probe light is picked up by a fiber beam splitter BS2 with a coupling ratio of 99.5:0.5, and the 400 kHz beat signal for the phase lock of the OPA is acquired with a PD5 using an avalanche photo diode (KPDEA007-T, Kyoto Semiconductor) followed by an amplification of $M = 10$. At the homodyne detector, since the LO light is not frequency-shifted, a beat signal of 200 kHz is observed, which is used for the phase lock of the homodyne detection. The beat signals obtained by the PD5 and the homodyne detector are demodulated as follows: To generate an error signal, the beat signal is mixed with the demodulation signal, and a second order low-pass filter is applied to it. To generate a feedback signal, the integration and proportional terms of PID feedback are activated. The feedback signals are fed back to the fiber stretchers (FSTs). The fiber stretchers have the following structure: A cube-shaped piezoelectric actuator PC4FL (Thorlabs) is sandwiched by two 25 mm-diameter semicircle metals, and a polarization-maintaining fiber is wound 10 times around it. The dynamic range of the fiber stretcher is about 3 wavelengths when the applied voltage range is set to 70 V. If the input polarization state deviates from the polarization-maintaining axis of the polarization-maintaining fiber, the polarization changes depending on the pressure on the fiber. Therefore, the fiber stretcher is placed immediately after the linear polarizer. The entire experimental system is covered by an airtight windshield made of aluminum frames, aluminum plates, and polycarbonate plates to suppress severe phase drifts due to temperature changes. The phase lock precision of the OPA was about 2°, and that of the homodyne detection was about 0.3°. The difference in the order of the phase lock accuracies is due to the difference in the amplitude of the signal between OPA and homodyne detection. Because the power of the LO light is much larger than that of the probe light, the signal-to-noise ratio of the homodyne detection is larger, and we can get a better measurement accuracy.

VII. POLARIZATION OPTIMIZATION

In Fig. 2, components that serve for the polarization optimizations are colored pink. First, the polarizations of the probe light before the OPA and the LO light are stabilized by linear polarizers (ILP-1550-900-1-0.5-SA-P30, Opneti) with the PER >30 dB. The polarizations of the probe light and the LO light after the linear polarizers are slightly changed unintentionally by the followed FST and BS1, which is critical in the squeezed light measurement. Therefore, we actively optimize the polarization using the fiber polarization controller PCD-M02 (LUNA), which can control polarization with three degrees of freedom.

The polarization optimization by feedback control is not a trivial problem. In the case of the LO, for instance, the feedback signal that goes to the polarization controller can be adjusted so that the amplitude of the interference signal is maximized. To investigate whether the current polarization state is optimized, the polarization state needs to be shifted slightly, and we need to check the decrease in the amplitude. Previous research implements polarization optimization by a random walk.[38] However, this random walk method is vulnerable to light power fluctuations, which cause amplitude fluctuations of the interference signal. Even if the polarization state is already in the optimal state, the control system may judge that the polarization is not optimal due to the power fluctuations and move from the current polarization state.

To solve this problem, we employed a polarization modulation method. By applying a modulation to the polarization and obtaining the error signal from the demodulation, it becomes possible to lock the polarization at the zero crosspoint of the error signal. Although the idea of applying the dither to the polarization is found in Ref. 21, the polarization stabilization is for classical light, which is insensitive

to optical losses. Thus, the light is picked up and sent to the polarizer to monitor the polarization. In the case of quantum light, which is sensitive to optical loss, we must limit the power picked up in order to minimize losses. Since we need to monitor the phase of the light as well as the polarization, it is better to share the light for the monitoring. Therefore, we do not insert the polarizer. In this experiment, we monitor the polarization of the light by the beat signal. For the phase-sensitive amplification in OPA, the polarization modulation is applied to the probe light. For the interference at BS-HD for homodyne detection, it is applied to the LO light.

A. Polarization modulation method

In this subsection, the polarization modulation method for the homodyne detection is mathematically described, and that for the OPA is described in Appendix A. The polarization modulation is turned on only during polarization alignment and off during squeezed light measurement. The on/off sequence of polarization control is described in Appendix B.

We are aiming to match the polarizations of the probe light and the LO light at BS-HD by the polarization modulation. Although the polarization of the probe light can change during the experiment, a polarization controller with a large loss should not be inserted in the path of the probe light through which the squeezed light is passing. Therefore, we put the polarization controller in the path of the LO light and aligned the polarization of the LO light to match that of the probe light. Note that we can instead insert a polarization controller with low optical loss to control the polarization of the squeezed light.[29]

The polarization is represented by a Poincaré sphere, where the radius of the Poincaré sphere is normalized by 1. Here, for simplicity, the polarization of the probe light and the LO light lie on a great circle that passes through the polarization V and the polarization R on the Poincaré sphere, as shown in Fig. 3. The polarization of the probe light is at the position rotated by $2\theta_1$ from the polarization V, and that of the LO light by $2\theta_2$. We assume the polarization controller can change the polarizations along this circle.[39] General situations of the polarizations are discussed later. The polarization modulation is applied by the polarization controller in the path of the LO light. The polarization modulation is expressed by $2A\sin(\omega_m t)$, where ω_m is the angular frequency of the polarization modulation and t is the time. The angular frequency of the LO light is ω_0, and the angular frequency of the probe light is shifted by $\Delta\omega$ from the LO light ($\Delta\omega$ corresponds to 200 kHz, which is mentioned in Sec. VI). Let the light travel along the z axis, and the polarization V of the Poincaré sphere corresponds to the x axis. Let $\mathbf{e}_x$ and $\mathbf{e}_y$ be unit vectors in the x and y axes, respectively. Assuming that the electric field amplitude is E_1 for the probe light and E_2 for the LO light. After they interfere with a polarization independent beam splitter with a coupling ratio of 50:50, the complex electric fields of two output beams $\boldsymbol{E}^{+}_{\mathrm{HD}}(t)$ and $\boldsymbol{E}^{-}_{\mathrm{HD}}(t)$ are

$$\begin{aligned}\boldsymbol{E}^{\pm}_{\mathrm{HD}}(t) = {} & \frac{1}{\sqrt{2}}E1(\cos\ \theta 1\mathbf{e}_x - i\ \sin\ \theta_1\mathbf{e}_y)\exp\left[-i(\omega_0+\Delta\omega)t + i\phi_1\right] \\ & \pm \frac{1}{\sqrt{2}}E_2\{\cos\left[\theta_2 + A\ \sin\left(\omega_m t\right)\right]\mathbf{e}_x \\ & - i\ \sin\left[\theta_2 + A\ \sin\left(\omega_m t\right)\right]\mathbf{e}_y\}\exp\left(-i\omega_0 t + i\phi_2\right), \end{aligned} \tag{1}$$

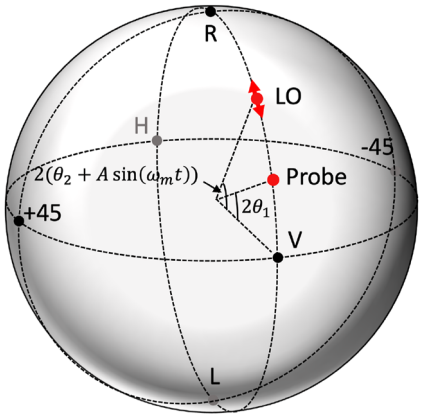

FIG. 3. Polarization of the probe light and the LO light on the Poincaré sphere in homodyne detection. The polarization modulation is applied only to the LO light. On the Poincaré sphere, R, L, V, H, +45, and −45 signs represent right-handed circular polarization, left-handed circular polarization, vertical linear polarization, horizontal linear polarization, linear polarization tilted by 45°, and linear polarization tilted by −45°, respectively. The right-handed and left-handed circular polarization are defined from the point of view of the receiver.

where ϕ_1 and ϕ_2 are the phases of the probe and LO light, respectively, which may drift during the experiments due to external disturbances. The signals that are obtained by the following photodiodes are

$$\begin{aligned}\left|\boldsymbol{E}^{\pm}_{\mathrm{HD}}(t)\right|^2 = {} & \frac{1}{2}E_1^2 + \frac{1}{2}E_2^2 \pm E_1E_2\ \cos\left[\theta_1 - \theta_2 - A\ \sin\left(\omega_m t\right)\right] \\ & \times \cos\left(-\Delta\omega t + \Delta\phi\right), \end{aligned} \tag{2}$$

where $\Delta\phi = \phi_1 - \phi_2$. With the homodyne detector, we measure the difference between the signals obtained from two photodiodes,

$$\begin{aligned}\left|\boldsymbol{E}^{+}_{\mathrm{HD}}(t)\right|^2 - \left|\boldsymbol{E}^{-}_{\mathrm{HD}}(t)\right|^2 = {} & 2E_1E_2\ \cos\left[\theta_1 - \theta_2 - A\ \sin\left(\omega_m t\right)\right] \\ & \times \cos\left(-\Delta\omega t + \Delta\phi\right), \end{aligned} \tag{3}$$

where the constant term is removed. Here, we assume $A \ll 1$ and use the following approximation:

$$\cos\left[\theta - A\ \sin\left(\omega_m t\right)\right] = \cos\ \theta + A\ \sin\left(2\theta\right)\sin\left(\omega_m t\right). \tag{4}$$

By applying the above approximation, Eq. (3) becomes

$$\begin{aligned}\left|\boldsymbol{E}^{+}_{\mathrm{HD}}(t)\right|^2 - \left|\boldsymbol{E}^{-}_{\mathrm{HD}}(t)\right|^2 = {} & 2E_1E_2[\cos\left(\theta_1 - \theta_2\right) + A\ \sin\left(\theta_1 - \theta_2\right) \\ & \times \sin\left(\omega_m t\right)]\cos\left(\Delta\omega t - \Delta\phi\right). \end{aligned} \tag{5}$$

From the above equation, the beat signal with the frequency $\Delta\omega$ is modulated at the frequency ω_m with a coefficient $A\sin(\theta_1 - \theta_2)$. Here, $\Delta\omega$ is chosen to be much higher than ω_m in order to remove the beat signal at the frequency of $\Delta\omega$.

There are two ways to remove the beat signal $\cos(\Delta\omega t - \Delta\phi)$. The first way is to multiply the $\cos(\Delta\omega t - \Delta\phi')$, which is externally generated,

$$\cos(\Delta\omega t - \Delta\phi)\cos(\Delta\omega t - \Delta\phi') = \frac{1}{2}\left[\cos(2\Delta\omega t - \Delta\phi - \Delta\phi') + \cos(-\Delta\phi + \Delta\phi')\right]. \quad (6)$$

The term angular frequency $2\Delta\omega$ is removed by the low-pass filter. However, the phase between $\Delta\phi$ and $\Delta\phi'$ needs to be synchronized to make this term constant. The other way is square-law detection, which is multiplying itself,

$$\cos^2(\Delta\omega t - \Delta\phi) = \frac{1}{2}\left[1 + \cos(2(\Delta\omega t - \Delta\phi))\right]. \quad (7)$$

In this way, we do not have to prepare a demodulation signal and synchronize the phase. Hence, in this experiment, we used a square-law detection.

Then ω_m is demodulated, and finally the error signal proportional to $\sin(\theta_1 - \theta_2)$ is obtained. This error signal is fed back to stabilize the polarization at $\theta_1 = \theta_2$. Note that Eq. (5) and Eq. (A5) in Appendix A are expressed in the same formula,

$$V_0(1 + \beta\cos(\Omega t))\cos(\omega_c t + \Delta\phi). \quad (8)$$

Here, β indicates how much the polarization deviates from the optimal polarization state ($\beta = 0$). The angular frequencies Ω and ω_c represent the angular frequency of the polarization modulation and the angular frequency of the beat signal, respectively. By extracting β, both polarizations at the OPA and the homodyne detection can be optimized in a similar manner.

So far we considered optimization in one degree of freedom, but the surface on the Poincaré sphere has two degrees of freedom. It is widely known that rotations around three axes are able to realize an arbitrary change in polarization. For example, the polarization controllers we used in this experiment have three piezo actuators in line: piezo 1, piezo 2, and piezo 3. Those piezo actuators apply pressure to a single-mode fiber (not a polarization maintaining fiber) and add retardation, which corresponds to the rotation around a certain axis on the Poincaré sphere. Piezo 2 is tilted by 45° relative to the others. This tilted piezo actuator introduces an additional axis of rotation on the Poincaré sphere, and this configuration enables an arbitrary polarization change.[39] The polarization modulation must be applied by the same piezo actuator used for the feedback control, and thus, polarization modulation is also switched in turn.

B. Implementation

Here, we describe the details of the demodulation circuit, including the parameters for the filters, and an algorithm to converge the polarization by three piezo actuators.

Since the polarization controllers used in this demonstration have a bandwidth of 2 kHz, the frequency of the polarization modulation is set to 300 Hz. This frequency is too low to demodulate by analog electric circuits. Therefore, we use an FPGA, which can easily implement many filters for low frequency signals. Furthermore, the parameters for the filters can be changed on site. Figure 4 shows the circuit configuration inside the FPGA to control the polarization of the LO light at the homodyne detection. Since the frequency of the probe light is shifted by 200 kHz, the interference between the probe light and the LO light generates a 200 kHz beat signal. In process 1, the 200 kHz signal is extracted by a bandpass filter to improve the signal-to-noise ratio of the beat signal. In process 2, square-law detection is applied to extract the power modulation component. After the signal is squared, the 400 kHz component is removed by a low-pass filter with a cutoff frequency of 30 kHz, and a high-pass filter with a cutoff frequency of 10 Hz is followed to remove the DC component. In process 3, the signal is demodulated at a polarization modulation frequency of 300 Hz to extract β in Eq. (8). The 300 Hz signal for the demodulation goes through a high-pass filter with a cutoff frequency of 10 Hz to remove the DC component, and then an all-pass filter to change the phase. Then the power modulation signal, which is obtained by process 2, is mixed with the 300-Hz demodulation signal. The DC component corresponds to β, while the second harmonic signal at 600 Hz is also generated. The 600 Hz signal is removed by a band-rejection filter, and the DC component is extracted by a low-pass filter with a cutoff frequency of 10 Hz. The sampling frequencies of the 200 kHz bandpass filter and the 30 kHz low-pass filter are 125 MHz, and those of other filters are downsampled to 1/16. The filter types are infinite response filters with second order.

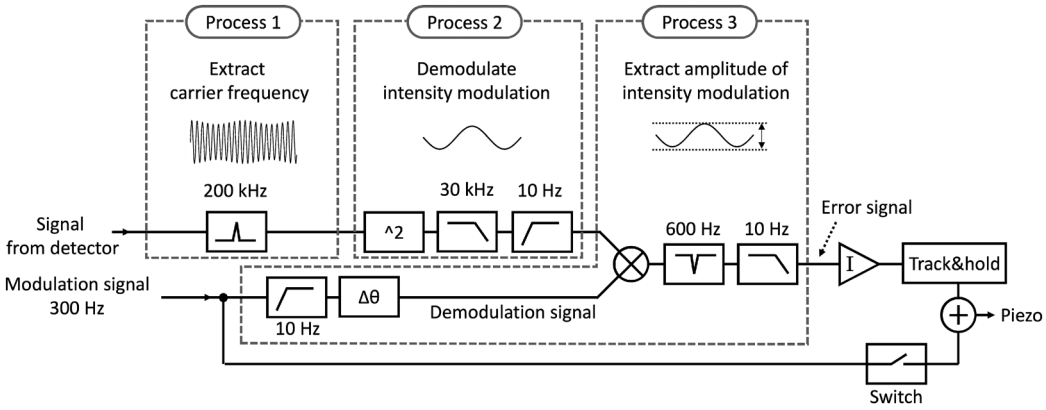

FIG. 4. Signal process inside the FPGA generates the error signal from the power modulation signal. Symbol I means integral of the error signal. The switch cut the modulation signal. After the optimization, the voltage applied to the piezo actuator is held (track and hold), and the modulation signal is cut.

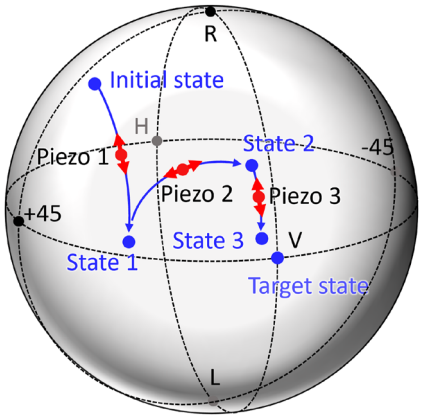

FIG. 5. Transition from the initial polarization state to the target polarization state using the polarization modulation method. Apply small polarization modulation to piezo 1, piezo 2, and piezo 3 in turn and adjust the offset applied to them so that the error signal approaches 0.

By the above process, the error signal β, which reflects a deviation from the optimum polarization state, is obtained. Then the error signal is fed back so that the error signal goes to zero. The 10-Hz cutoff frequency of the last low-pass filters is sufficient as a feedback bandwidth for polarization control because the polarizations vary slowly in the order of several tens of minutes caused by the ambient temperature change.

The filter bandwidths are designed by choosing the parameters for the infinite response filter. We verified the bandwidth by a network analyzer, which sends a sinewave swept in the target frequency range and records the response. The bandwidths of the implemented filters agree well with the expected values.

The piezo actuators inside the polarization controllers, to which the polarization modulation and the control signal are applied, accept the voltage range from 0 to 140 V. If the digital input mode is selected, that voltage range corresponds to the integer range from 0 to 4095. The amplitude of the polarization modulation is set to 32.

The three piezo actuators are controlled in turn, as shown in Fig. 5. First, piezo 1 is vibrated to apply the polarization modulation, and the obtained error signal β_1 is integrated and then sent back to piezo 1. When the error signal becomes close to zero, the feedback and the vibration of piezo 1 are terminated. At this time, the polarization changes from the initial state to state 1. Next, similarly, piezo 2 is driven, and the obtained error signal β_2 is processed, resulting in the polarization change from state 1 to state 2. Then, piezo 3 and β_3 go in the same manner, resulting in the polarization change from state 2 to state 3. This process is cyclically repeated from piezo 1 to piezo 3 for several cycles to converge to the target state. Note that, since the polarization state may converge to the state opposite to the optimum depending on the initial state, the initial state should be manually set near the optimum.

C. Comparison

We made an experiment to compare the polarization modulation method with the random walk method. The initial state is set to the optimum polarization state by hand, and the polarization optimization is performed with 1000 feedback steps at a rate of 30 steps/s. Figure 6 shows the digital values sent to the three piezo actuators (piezo 1, piezo 2, and piezo 3) for the random walk method (red) and the polarization modulation method (blue). Since the polarization state changes in the order of several tens of minutes, the polarization is expected to be stable in this measurement time scale (33 s). Even though the initial state is optimal, there are undesirable changes of the digital values for the random walk method. This is because, when the polarization is close to the optimum, slight power fluctuations degrade the stability of the random walk method, as already mentioned. On the other hand, the additional polarization drifts are not induced by the polarization modulation method.

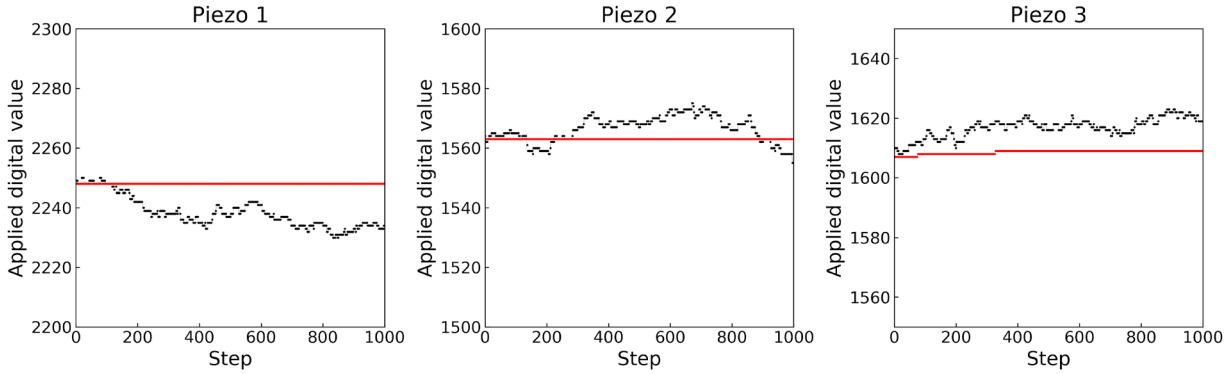

FIG. 6. Change in digital values sent to the three piezo actuators (piezo 1, piezo 2, and piezo 3) when polarization optimization is performed with the random walk method (gray) and the polarization modulation method (red) for 1000 steps at 30 steps/s. In this figure, the traces for the polarization modulation method are the digital values, which do not contain the modulation. The initial state is manually set to be the optimum polarization state. Since the polarization states fluctuate in the order of several tens of minutes, the digital values should not move in this time scale. For the random walk method, digital values are constantly fluctuating. On the other hand, for the polarization modulation method, they are stable.

VIII. BEAM SPLITTER COUPLING RATIO LOCK

Before explaining the beam splitter coupling ratio lock, we refer to the structures of the beam splitter. The beam splitters are directional couplers, and light is exchanged between two fibers by evanescent coupling. Fiber beam splitters are basically classified into two types: fused biconical tapered couplers[40,41] and side polished couplers.[42,43] For the fused biconical tapered coupler, two fibers are twisted together and stretched on heating. In this method, the deformation of the cores results in the high optical loss. On the other hand, for the side-polished coupler, fibers are embedded in quartz substrates. Next, some part of the cladding is polished until it is removed to permit the evanescent coupling. Then the two pieces are contacted. In this method, the cores are not deformed, resulting in lower optical loss. To reduce the optical loss of squeezed light, we use side-polished fiber beam splitters for the quantum light paths (BS2 and BS-HD in this demonstration).

In addition to the low-loss demand, the coupling ratio of the beam splitter at the homodyne detection (BS-HD) must be exactly 50:50 for the following reason: In homodyne detection, the LO light interferes with the squeezed light and is divided at BS-HD. Then the difference between two photocurrents is electrically amplified, and the residual fluctuation represents the quadrature phase amplitude. Because the power of the LO light is very high, the unbalance of the two photocurrents caused by a slight deviation of the coupling ratio from 50:50 easily results in saturation of the homodyne detector. In addition, since the DC output of the homodyne detector is used for generating various error signals as shown in Fig. 2, we do not want to make the homodyne detector AC coupled to prevent saturation.

The coupling ratio is required to be 50:50 with an accuracy of less than 0.1% from the following experimental parameters. The LO power is 16 mW and the probe power is 1 μW. The difference of the two photocurrents is converted to a voltage by a transimpedance amplifier with a feedback resistance of 3.03 kΩ, and then further amplified by 15 times. The output voltage of the detector should be kept in the range from −1 to 1 V to avoid saturation of the op-amp.

We use a custom-made fiber beam splitter, 905P (Evanescent Optics), whose coupling ratio can be changed by a micrometer. However, some obstacles are found for the stabilization of the coupling ratio. First, the response of the coupling ratio has a hysteresis and a backlash for the micrometer displacement, as shown in Fig. 7. Even if we do not have to consider the hysteresis of the coupling ratio

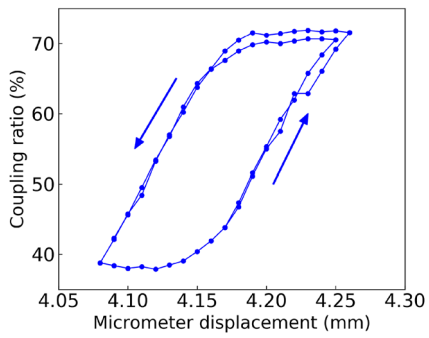

FIG. 7. Hysteresis of the coupling ratio depending on the micrometer displacement.

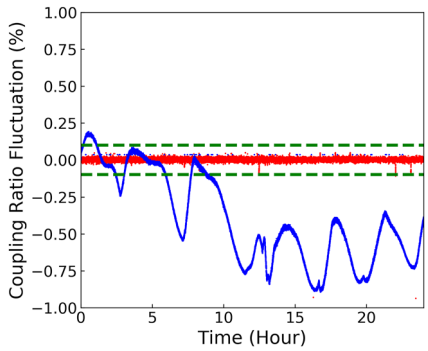

FIG. 8. Change in the coupling ratio of the fiber beam splitter measured over 24 h. Red: results when the homodyne signal is fed back to the Peltier element. Blue: results when the temperature measured by the thermistor is fed back to the Peltier element. Green: lines at the level of ±0.1%, where the homodyne detector does not saturate in this study. The standard deviation of the coupling ratio is 0.01% for the red trace.

depending on the micrometer, to control the coupling ratio to 50% with the accuracy of 0.1%, the micrometer displacement should be adjusted with the accuracy of 0.27 μm. It is hard to achieve this accuracy. Second, it takes about 6 min for the coupling ratio to be stable after the user takes his or her hand off the knob. Third, for the beam splitter used in this study, the coupling ratio has a dependency on the temperature at a rate of 0.95%/°C around the coupling ratio of 50:50. Fourth, the coupling ratio changes by about 2.9% depending on the polarization state of the input light. Therefore, it is hard to maintain the coupling ratio with an accuracy of 0.1%. We note that the above properties vary on each fiber beam splitter.

To stabilize the coupling ratio of the beam splitter, we use the temperature as a degree of freedom for control. We attach a Peltier element to the bottom of the beam splitter and a thermistor to the side of the beam splitter and place them on a heat sink. As a first test, we controlled the temperature measured by the thermistor to be kept constant. After 24 h, the coupling ratio varied by about 1%, as shown in Fig. 8 (blue line), which was worse than the acceptable coupling ratio deviation of 0.1%. Therefore, we employ a method to stabilize the coupling ratio of the beam splitter by monitoring the drift of the average of the homodyne detection signal and by feeding it back to the Peltier element. As shown in Fig. 8 (red line), the coupling ratio fluctuation is locked with a standard deviation of 0.01% for 24 h, which is sufficiently smaller than the target fluctuation of 0.1%. When the coupling ratio is shifted for the first time, it takes a couple of minutes to stabilize. Although this method uses temperature dependence of the fiber beam splitter, some fiber beam splitters have little temperature dependence. Therefore, it is necessary to select those that have a sufficient temperature dependence or to develop a fiber beam splitter with a structure that has enough temperature dependence.

IX. 24-h SQUEEZED LIGHT MEASUREMENT

Squeezed light is measured for 24 h in the fiber system using various stabilization mechanisms explained above. 24 h is enough. As described in Appendix B, the alignments and the squeezed light

measurements are repeated alternately in this experiment, with various controllers turned on and off in sequence. The spectra of the squeezing and antisqueezing levels in the range from 10 to 200 MHz are acquired with a resolution bandwidth of 1 MHz and a video bandwidth of 10 Hz by a spectrum analyzer PXA Signal Analyzer N9030B (Keysight).

Figure 9(a) shows time variations of squeezing level and antisqueezing level at 40 MHz as blue and red points, respectively. As a reference, an example of the squeezing level and antisqueezing level are shown as sky blue and pink points, respectively, for the case where the polarization stabilizations and coupling ratio lock of the beam splitter are deactivated. Note that the phase locks and the power stabilizations are active for obtaining the sky blue and pink points. The blue and red points are obtained every 2 min, and the sky blue and pink points every 11 min. The blue points show an average squeezing level of −4.42 dB with an extremely small standard deviation of ±0.08 dB over 24 h. The red points show an average antisqueezing level of 7.85 dB with a standard deviation of 0.13 dB. In contrast, for the sky blue points, the squeezing level is not kept as the time passes. These results demonstrate that stabilization controls work properly to keep the system stable. Without the automated alignment, the squeezing level degrades in a couple of hours. Therefore, to confirm the improvement with the automated alignment, we believe 24 h (1 day) are sufficient. Note that squeezing and antisqueezing levels have some outliers because they are not measured properly for the following reasons: When the phase drift exceeds the dynamic range of the fiber stretcher, the voltage applied to the fiber stretcher is reset and the phase is relocked. If squeezed light measurements coincide with the reset process, inappropriate squeezing or antisqueezing levels are obtained. This problem can be prevented by programming the control system, but we did not implement it in this measurement. When the average and the standard deviation of the squeezing and antisqueezing levels are calculated, these outliers are omitted.

We can estimate the effective loss of the system from the squeezing level and antisqueezing level. In addition to the insertion losses of optical components, the polarization mismatches become effective losses for the squeezed light, which reduces the squeezing level. If the change in the effective loss of the system is small, we can verify that the polarization matching is stable during the measurement. Figure 9(b) shows the effective loss of the entire system estimated from the blue and red points in Fig. 9(a). From the

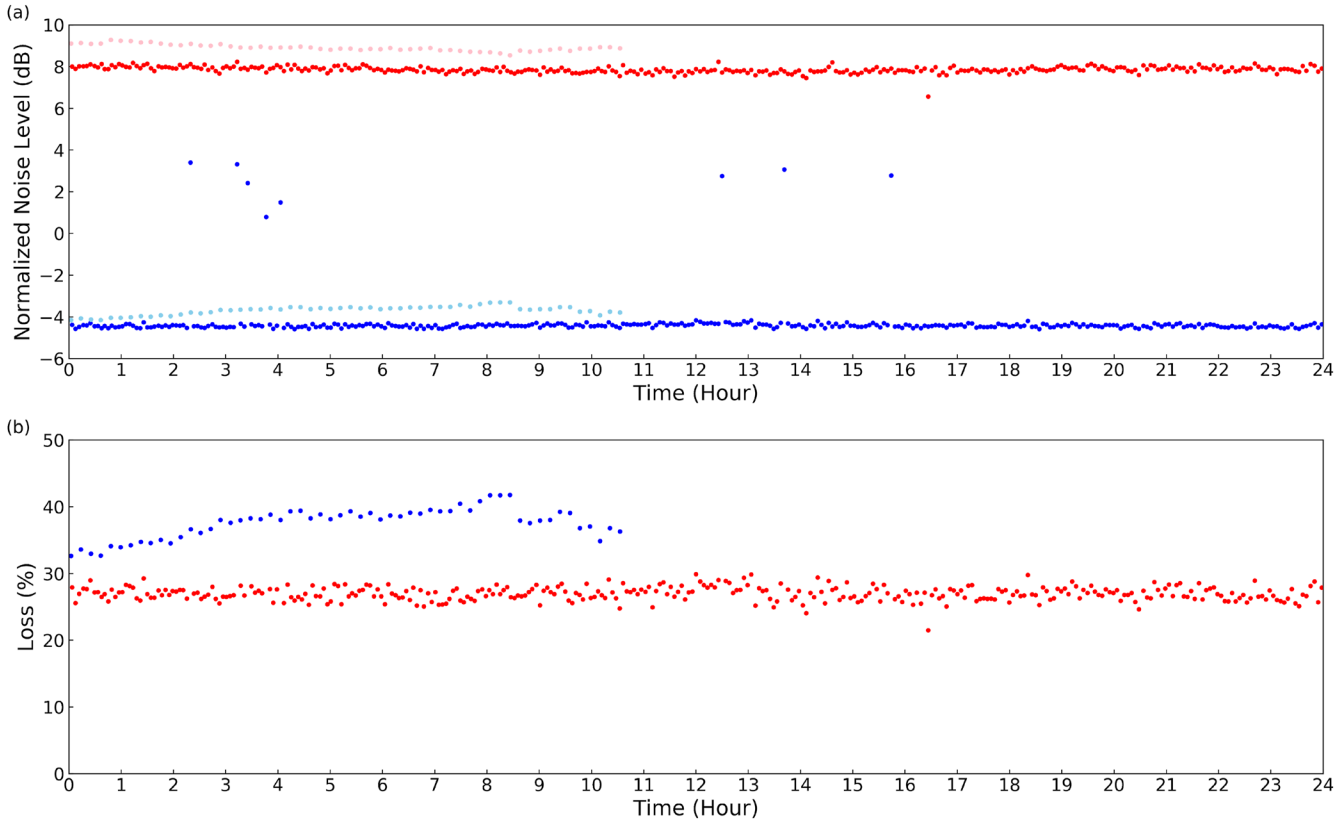

FIG. 9. Results of 24-h squeezed light measurement. (a) Time variation of the squeezing and antisqueezing levels. Blue: squeezing level. Red: antisqueezing level. The sky blue: squeezing and pink: antisqueezing levels are collected with the polarization stabilization and coupling ratio control deactivated, while the power stabilization and phase locks remain active. (b) Time variation of the effective loss of the entire experimental system. Red: loss with full control. Blue: loss with the same control configuration used for the sky blue and pink traces in (a).

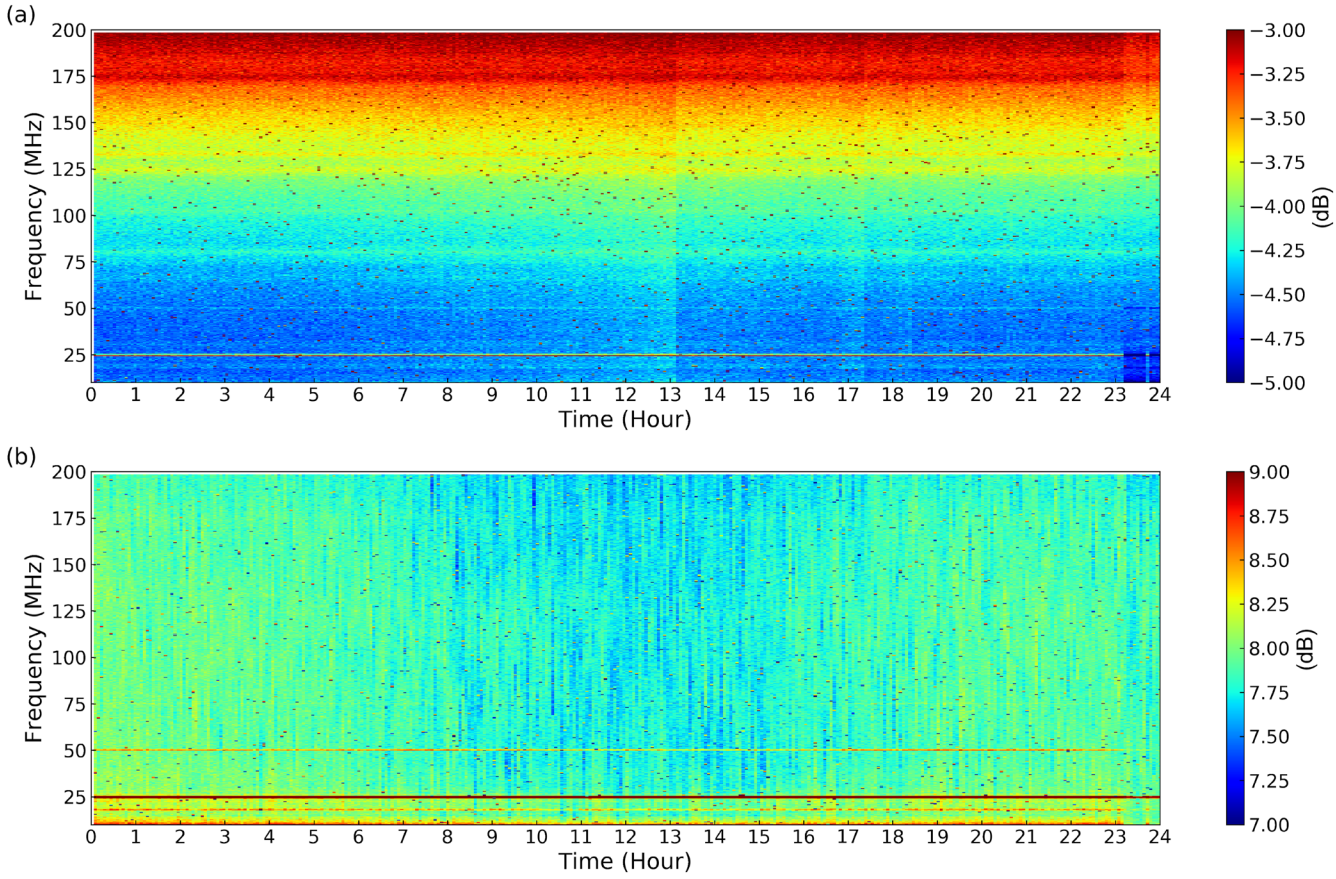

FIG. 10. Spectrogram from 10 to 200 MHz for 24-h squeezed measurements. (a) Squeezing level. (b) Antisqueezing level.

squeezing level sq and antisqueezing level asq expressed in dB, we can evaluate the effective loss L of the whole system from the following relations:

$$sq = 10\log_{10}(L + (1-L)e^{-2r}), \tag{9}$$

$$asq = 10\log_{10}(L + (1-L)e^{2r}), \tag{10}$$

where $r \geq 0$ is the squeezing parameter. In the ideal case where a loss is absent, the squeezing and antisqueezing levels become symmetric ($sq = -asq$). In actual cases where a loss exists, a vacuum fluctuation is mixed to the squeezed or antisqueezed quadrature, from which the above equations are derived. From the above equations, L is expressed as

$$L = \frac{1 - 10^{\frac{sq}{10}} + \frac{asq}{10}}{2 - 10^{\frac{sq}{10}} - 10^{\frac{asq}{10}}}. \tag{11}$$

The time variation of effective loss was calculated to be 27.0 ± 1.0%, as shown in Fig. 9(b). The fact that the loss fluctuation was only ±1.0% over 24 h demonstrates that the control system is operating stably for a long period. The details of the 27% loss are as follows: The loss of the OPA is from 8% to 12%. Two connectors are used, where the loss of each connector is from 3% to 5%. The loss of BS2 is about 3%. The loss of BS-HD is about 0.5%. The loss of the homodyne detection device is about 4%. As an option, the connectors can be fused, by which the loss is reduced to 0.5% per one connection point. In this experiment, fusion splicing is not done for the reusability of the OPA.

Figure 10 shows a spectrogram of the squeezing and antisqueezing levels. The dots in Fig. 10 are due to the same reason for the phase re-locking as in Fig. 9. The line at 25 MHz is due to electric noise.

X. CONCLUSION

In this study, squeezed light with a squeezing level of −4.42 dB has been successfully generated and measured in a fiber-based experimental system with a very small standard deviation of ±0.08 dB for 24 h. Squeezed light is the most fundamental quantum state of light in cluster quantum computations[4–14] and loop quantum computations.[44,45] In the case of the free space experimental setup, as the system size gets larger, it becomes harder to keep it stable. On the contrary, there are no limitations in the case of the fiber system if we

employ the technology demonstrated in this paper. Therefore, generating a complicated cluster state is realistic with the fiber system. Furthermore, the system, which can be automatically kept stable for long periods of time, enables reliable operations of optical quantum computers offered as a cloud service.

ACKNOWLEDGMENTS

This work was partly supported by Japan Science and Technology Agency (Moonshot R&D) Grant Nos. JPMJMS2064 and JPMJPR2254, Japan Society for the Promotion of Science KAKENHI Grant Nos. 18H05207 and 20K15187, the UTokyo Foundation, and donations from Nichia Corporation of Japan. T.N. acknowledges the financial support from the Forefront Physics and Mathematics Program to Drive Transformation (FoPM). M.E. acknowledges the support from the Research Foundation for Opto-Science and Technology.

AUTHOR DECLARATIONS

Conflict of Interest

The authors have no conflicts to disclose.

Author Contributions

Tomohiro Nakamura: Data curation (equal); Formal analysis (equal); Investigation (equal); Methodology (equal); Visualization (equal); Writing – original draft (equal); Writing – review & editing (equal). **Takefumi Nomura**: Writing – review & editing (supporting). **Mamoru Endo**: Methodology (supporting); Writing – original draft (supporting); Writing – review & editing (supporting). **Atsushi Sakaguchi**: Writing – review & editing (supporting). **He Ruofan**: Writing – review & editing (supporting). **Takahiro Kashiwazaki**: Writing – review & editing (supporting). **Takeshi Umeki**: Writing – review & editing (supporting). **Kan Takase**: Writing – review & editing (supporting). **Warit Asavanant**: Writing – review & editing (supporting). **Jun-ichi Yoshikawa**: Conceptualization (supporting); Methodology (supporting); Supervision (supporting); Visualization (supporting); Writing – original draft (supporting); Writing – review & editing (supporting). **Akira Furusawa**: Project administration (equal); Writing – review & editing (equal).

DATA AVAILABILITY

The data that support the findings of this study are available from the corresponding author upon reasonable request.

APPENDIX A: POLARIZATION MODULATION AT THE OPA

Here, we mathematically describe the polarization modulation method at the OPA. We aim to match the polarization of the probe light to the crystal axis where parametric downconversion happens. The crystal axis is set to the x axis, which corresponds to the polarization V in the Poincaré sphere. In a similar manner to Sec. VII, for simplicity, let us consider the situation where the polarization of the input probe light is shifted from the polarization V to the polarization R by 2θ, as shown in Fig. 11. In this case, we aim to control θ to be 0. The polarization of the probe light input to the OPA is slightly modulated on the Poincaré sphere by $2A\sin(\omega_m t)$, where A is the amplitude of the polarization modulation ($A \ll 1$), ω_m is the angular frequency of polarization modulation, and t is the time. The optical angular frequency of the degenerate parametric down-conversion is denoted by ω_0, the frequency shift of the probe light from the degenerate frequency $\Delta\omega$, the electric field amplitude E_0, and the optical phase of probe light ϕ. Then the complex electric field of the probe light input to OPA $\boldsymbol{E}_{\text{beforeOPA}}$ is

$$\begin{aligned}\boldsymbol{E}_{\text{beforeOPA}} = E_0\{&\cos[\theta + A\sin(\omega_m t)]\mathbf{e}_x - i\sin[\theta + A\sin(\omega_m t)]\mathbf{e}_y\}\\ &\times \exp[-i(\omega_0 + \Delta\omega)t + i\phi_{\text{probe}}].\end{aligned} \tag{A1}$$

Only the polarization element of the probe light parallel to the crystal axis of a nonlinear crystal undergoes phase-sensitive amplification, while the perpendicular element remains unchanged. If the degrees of the phase-sensitive amplification is $\exp(r)$ and the phase of the pump light is ϕ_{pump}, the electric field $\boldsymbol{E}_{\text{afterOPA}}$ of the probe light output from the OPA is[46]

$$\begin{aligned}\boldsymbol{E}_{\text{afterOPA}} = E_0&\cos[\theta + A\sin(\omega_m t)]\\ &\times\{\cosh(r)\exp[-i(\omega_0 + \Delta\omega)t + i\phi_{\text{probe}}]\\ &+ i\sinh(r)\exp[-i(\omega_0 - \Delta\omega)t - i\phi_{\text{probe}} + i\phi_{\text{pump}}]\}\mathbf{e}_x\\ &- iE_0\sin[\theta + A\sin(\omega_m t)]\exp[-i(\omega_0 + \Delta\omega)t + i\phi_{\text{probe}}]\mathbf{e}_y.\end{aligned} \tag{A2}$$

The intensity of light I is proportional to the square of the electric field,

$$\begin{aligned}I \propto |\boldsymbol{E}_{\text{afterOPA}}|^2 = E_0^2\{&\cos^2[\theta + A\sin(\omega_m t)]\times[\cosh(2r) + \sinh(2r)\\ &\times\sin(2\Delta\omega t - 2\phi_{\text{probe}} + \phi_{\text{pump}})]\\ &+ \sin^2[\theta + A\sin(\omega_m t)]\}.\end{aligned} \tag{A3}$$

From $A \ll 1$, the following approximation is obtained:

$$\cos^2[\theta + A\sin(\omega_m t)] = \cos^2\theta - A\sin(2\theta)\sin(\omega_m t). \tag{A4}$$

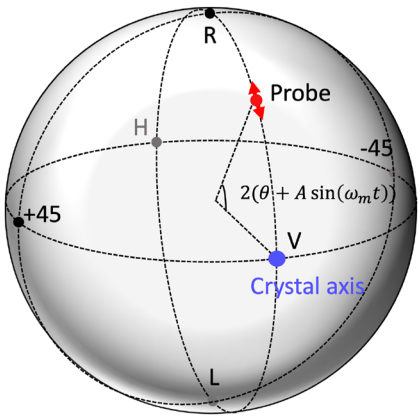

FIG. 11. Polarization on the Poincaré sphere of the probe light with polarization modulation before the OPA.

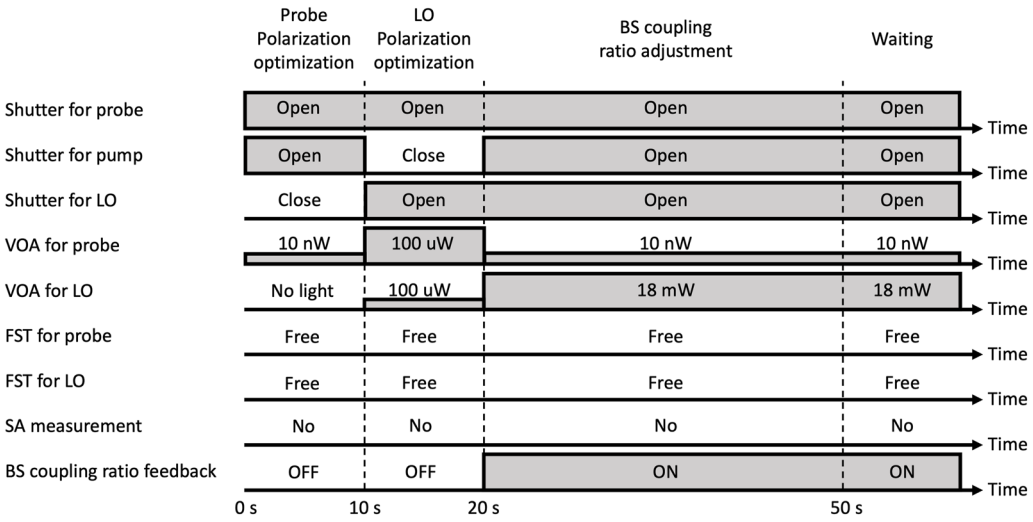

FIG. 12. Alignment sequence performed every 30 min.

By using the above expression, the element oscillating at angular frequency $2\Delta\omega$ in Eq. (A3), which is extracted by BPF, is

$$E_0^2[\cos^2\theta - A\,\sin(2\theta)\sin(\omega_m t)]\sinh(2r)$$
$$\sin(2\Delta\omega t - 2\phi_{\text{probe}} + \phi_{\text{pump}}). \quad \text{(A5)}$$

The signal with the angular frequency of $2\Delta\omega$ is intensity modulated at an angular frequency of ω_m. Intensity modulation is extracted by the square-law detection, where we can neglect the phase drift $-2\phi_{\text{probe}} + \phi_{\text{pump}}$, as explained in Sec. VII. The intensity modulation element is proportional to $\sin(2\theta)$, which is exacted by a demodulation at the frequency of ω_m. By using $\sin(2\theta)$, we can control the polarization to $\theta = 0$ or $\theta = \pi/2$, which depends on the polarity of the feedback.

The angular frequency of the carrier signal is $2\Delta\omega$ for the OPA as shown in Eq. (A5), while $\Delta\omega$ for the homodyne detection as shown in Eq. (5). Thus, for the cascade filter implemented by FPGA, the center frequency of the BPF in Process 1 is 400 kHz for the OPA, while 200 kHz for the homodyne detection.

APPENDIX B: SEQUENCE FOR ALIGNMENT AND MEASUREMENT

In this demonstration, automatic alignment is performed once every 30 min, and squeezed light measurement is performed once every 2 min. Alignment is conducted by the sequence in Fig. 12. First, to match the polarization of the probe light and the crystal axis of the PPLN, only the probe and the pump light go through the shutter, polarization modulation is applied to the probe light, and polarization control is performed using a beat signal of 400 kHz. Then, to match the polarization of the probe and the LO light, only

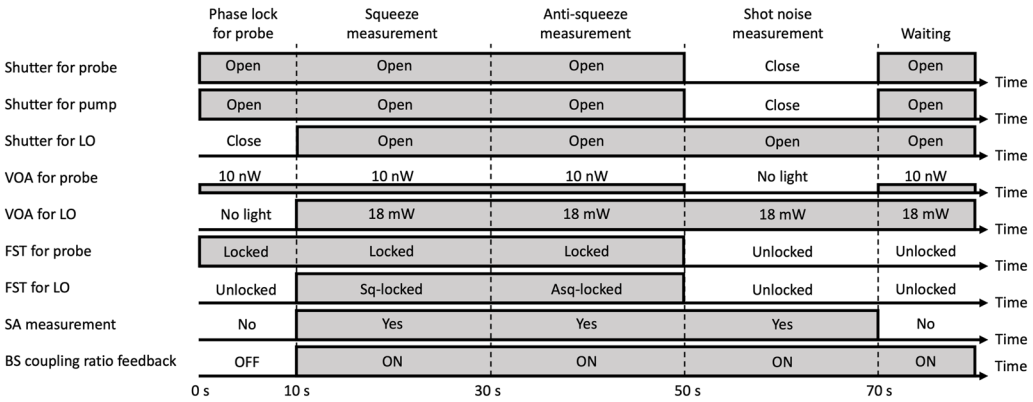

FIG. 13. Squeezed light measurement sequence performed every 2 min.

the probe and the LO light go through the shutter, polarization modulation is applied to the LO light only, and polarization control is performed using a beat signal of 200 kHz. Since the coupling ratio of the beam splitter for homodyne measurement slightly depends on the polarization of the input light, control of the coupling ratio is assigned after polarization control of the probe and the LO light. During the above alignment, the fiber stretcher is fixed at a constant voltage (unlocked).

Squeezed light measurements are performed in the sequences shown in Fig. 13. First, the phase of the probe light is locked with respect to the pump light. When the pump light is input, the temperature of the PPLN inside the OPA increases, and the phase drift occurs for a while. Therefore, we wait for 10 s so that it settles down. Next, the phase of the LO light is locked with respect to the probe light, and the squeezing and antisqueezing levels are measured. Finally, for the shot noise level measurement, all phase locks are released and only the LO light is input. During measurement time, control of the coupling ratio of the beam splitter is activated.

With this sequence, the squeezed light is periodically stopped to align the system. However, for the continuous variable quantum computation, continuously generated squeezed light is necessary. Actually, the periodical alignment is inserted every couple of minutes. On the other hand, the clock period of quantum mode reported so far is less than 1 μs.[8,9,12,13] Therefore, periodic alignment does not limit the ability of quantum computation.

REFERENCES

[1] L. Egan, D. M. Debroy, C. Noel, A. Risinger, D. Zhu, D. Biswas, M. Newman, M. Li, K. R. Brown, M. Cetina, and C. Monroe, "Fault-tolerant control of an error-corrected qubit," Nature **598**, 281–286 (2021).

[2] See https://research.ibm.com/blog/127-qubit-quantum-processor-eagle for IBM Quantum breaks the 100-qubit processor barrier.

[3] L. S. Madsen, F. Laudenbach, M. F. Askarani, F. Rortais, T. Vincent, J. F. F. Bulmer, F. M. Miatto, L. Neuhaus, L. G. Helt, M. J. Collins, A. E. Lita, T. Gerrits, S. W. Nam, V. D. Vaidya, M. Menotti, I. Dhand, Z. Vernon, N. Quesada, and J. Lavoie, "Quantum computational advantage with a programmable photonic processor," Nature **606**, 75–81 (2022).

[4] R. Raussendorf and H. J. Briegel, "A one-way quantum computer," Phys. Rev. Lett. **86**, 5188–5191 (2001).

[5] N. C. Menicucci, P. van Loock, M. Gu, C. Weedbrook, T. C. Ralph, and M. A. Nielsen, "Universal quantum computation with continuous-variable cluster states," Phys. Rev. Lett. **97**, 110501 (2006).

[6] N. C. Menicucci, "Temporal-mode continuous-variable cluster states using linear optics," Phys. Rev. A **83**, 062314 (2011).

[7] M. Pysher, Y. Miwa, R. Shahrokhshahi, R. Bloomer, and O. Pfister, "Parallel generation of quadripartite cluster entanglement in the optical frequency comb," Phys. Rev. Lett. **107**, 030505 (2011).

[8] S. Yokoyama, R. Ukai, S. C. Armstrong, C. Sornphiphatphong, T. Kaji, S. Suzuki, J. I. Yoshikawa, H. Yonezawa, N. C. Menicucci, and A. Furusawa, "Ultra-large-scale continuous-variable cluster states multiplexed in the time domain," Nat. Photonics **7**, 982–986 (2013).

[9] J. I. Yoshikawa, S. Yokoyama, T. Kaji, C. Sornphiphatphong, Y. Shiozawa, K. Makino, and A. Furusawa, "Invited Article: Generation of one-million-mode continuous-variable cluster state by unlimited time-domain multiplexing," APL Photonics **1**, 060801 (2016).

[10] R. Yang, J. Wang, J. Zhang, K. Liu, and J. Gao, "Generation of continuous-variable spatial cluster entangled states in optical mode comb," J. Opt. Soc. Am. B **33**, 2424 (2016).

[11] J. Zhang, J. J. Wang, R. G. Yang, K. Liu, and J. R. Gao, "Large-scale continuous-variable dual-rail cluster entangled state based on spatial mode comb," Opt. Express **25**, 27172 (2017).

[12] M. V. Larsen, X. Guo, C. R. Breum, J. S. Neergaard-nielsen, and U. L. Andersen, "Deterministic generation of a two-dimensional cluster state," Science **366**, 369–372 (2019).

[13] W. Asavanant, Y. Shiozawa, S. Yokoyama, B. Charoensombutamon, H. Emura, R. N. Alexander, S. Takeda, J. I. Yoshikawa, N. C. Menicucci, H. Yonezawa, and A. Furusawa, "Generation of time-domain-multiplexed two-dimensional cluster state," Science **366**, 373–376 (2019).

[14] O. Pfister, "Continuous-variable quantum computing in the quantum optical frequency comb," J. Phys. B: At., Mol. Opt. Phys. **53**, 012001 (2020).

[15] M. Tur, Y. S. Boger, and H. J. Shaw, "Polarization-induced fading in fiber-optic sensor arrays," J. Lightwave Technol. **13**, 1269–1276 (1995).

[16] R. Slavík, G. Marra, E. N. Fokoua, N. Baddela, N. V. Wheeler, M. Petrovich, F. Poletti, and D. J. Richardson, "Ultralow thermal sensitivity of phase and propagation delay in hollow core optical fibres," Sci. Rep. **5**, 15447 (2015).

[17] Y. Lv, P. Wang, Y. Wang, X. Liu, Q. Bai, P. Li, H. Zhang, Y. Gao, and B. Jin, "Eliminating phase drift for distributed optical fiber acoustic sensing system with empirical mode decomposition," Sensors **19**, 5392 (2019).

[18] R. Ulrich, "Polarization stabilization on single-mode fiber," Appl. Phys. Lett. **35**, 840–842 (1979).

[19] T. Okoshi, "Polarization-state control schemes for heterodyne or homodyne optical fiber communications," IEEE Trans. Electron Devices **32**, 2624–2629 (1985).

[20] A. D. Kersey, M. J. Marrone, A. Dandridge, and A. B. Tveten, "Optimization and stabilization of visibility in interferometric fiber-optic sensors using input-polarization control," J. Lightwave Technol. **6**, 1599–1609 (1988).

[21] F. Heismann and M. S. Whalen, "Fast automatic polarization control system," IEEE Photonics Technol. Lett. **4**, 503–505 (1992).

[22] W. Shieh and H. Kogelnik, "Dynamic eigenstates of polarization," IEEE Photonics Technol. Lett. **13**, 40–42 (2001).

[23] N. Ming, Y. Hua-yong, X. Shui-dong, and H. Yong-ming, "Investigation of polarization-induced fading in fiber-optic interferometers with polarizer-based polarization diversity receivers," Appl. Opt. **45**, 2387–2390 (2006).

[24] M. Martinelli, P. Martelli, and S. M. Pietralunga, "Polarization stabilization in optical communications systems," J. Lightwave Technol. **24**, 4172–4183 (2006).

[25] H. Lin, L. Ma, Y. Hu, and W. Wang, "Elimination of polarization-induced signal fading and reduction of phase noise in interferometric optical fiber sensor using polarization diversity receivers," Optik **124**, 4976–4979 (2013).

[26] Q. Chen, T. Liu, K. Liu, J. Jiang, Z. Ding, L. Zhang, Y. Li, L. Pan, and C. Ma, "An elimination method of polarization-induced phase shift and fading in dual Mach-Zehnder interferometry disturbance sensing system," J. Lightwave Technol. **31**, 3135–3141 (2013).

[27] T. Kashiwazaki, N. Takanashi, T. Yamashima, T. Kazama, K. Enbutsu, R. Kasahara, T. Umeki, and A. Furusawa, "Continuous-wave 6-dB-squeezed light with 2.5-THz-bandwidth from single-mode PPLN waveguide," APL Photonics **5**, 036104 (2020).

[28] T. Kashiwazaki, T. Yamashima, K. Enbutsu, T. Kazama, A. Inoue, K. Fukui, M. Endo, T. Umeki, and A. Furusawa, "Over-8-dB squeezed light generation by a broadband waveguide optical parametric amplifier toward fault-tolerant ultra-fast quantum computers," Appl. Phys. Lett. **122**, 234003 (2023).

[29] T. Nakamura, T. Nomura, M. Endo, R. He, T. Kashiwazaki, T. Umeki, J.-i. Yoshikawa, and A. Furusawa, "Low-loss polarization control in fiber systems for quantum computation," Opt. Express **31**, 19236–19254 (2023).

[30] N. Takanashi, T. Kashiwazaki, T. Kazama, K. Enbutsu, R. Kasahara, T. Umeki, and A. Furusawa, "4-dB quadrature squeezing with fiber-coupled PPLN ridge waveguide module," IEEE J. Quantum Electron. **56**, 6000100 (2020).

[31] C. Nguyen, M. Bawaj, V. Sequino, M. Barsuglia, M. Bazzan, E. Calloni, G. Ciani, L. Conti, B. D'Angelo, R. De Rosa, L. Di Fiore, S. Di Pace, V. Fafone, B. Garaventa, A. Gennai, L. Giacoppo, I. Khan, M. Leonardi, E. Majorana, L. Naticchioni, F. Paoletti, D. Passuello, M. Pegoraro, F. Ricci, A. Rocchi, M. Vardaro, H. Vocca,

J.-P. Zendri, M. De Laurentis, and F. Sorrentino, "Automated source of squeezed vacuum states driven by finite state machine based software," Rev. Sci. Instrum. **92**, 054504 (2021).
[32]B. Shajilal, O. Thearle, A. Tranter, Y. Lu, E. Huntington, S. Assad, P. K. Lam, and J. Janousek, "12.6 dB squeezed light at 1550 nm from a bow-tie cavity for long-term high duty cycle operation," Opt. Express **30**, 37213 (2022).
[33]U. L. Andersen, T. Gehring, C. Marquardt, and G. Leuchs, "30 Years of squeezed light generation," Phys. Scr. **91**, 053001 (2016).
[34]N. C. Menicucci, "Fault-tolerant measurement-based quantum computing with continuous-variable cluster states," Phys. Rev. Lett. **112**, 120504 (2014).
[35]K. Fukui, A. Tomita, A. Okamoto, and K. Fujii, "High-threshold fault-tolerant quantum computation with analog quantum error correction," Phys. Rev. X **8**, 021054 (2018).
[36]H. Vahlbruch, M. Mehmet, K. Danzmann, and R. Schnabel, "Detection of 15 dB squeezed states of light and their application for the absolute calibration of photoelectric quantum efficiency," Phys. Rev. Lett. **117**, 110801 (2016).
[37]M. S. Elezov, M. L. Scherbatenko, D. V. Sych, and G. N. Goltsman, "Active and passive phase stabilization for the all-fiber Michelson interferometer," J. Phys.: Conf. Ser. **1124**, 051014 (2018).
[38]S. C. Huang, "Automatic polarization compensation tracking method for maximum visibility of fiber interferometric sensors," J. Lightwave Technol. **27**, 4040–4048 (2009).
[39]Y. Shi, L. Yan, and X. S. Yao, "Automatic maximum–minimum search method for accurate PDL and DOP characterization," J. Lightwave Technol. **24**, 4006–4012 (2006).
[40]B. S. Kawasaki, K. O. Hill, and R. G. Lamont, "Biconical-taper single-mode fiber coupler," Opt. Lett. **6**, 327 (1981).
[41]B. P. Pal, P. R. Chaudhuri, and M. R. Shenoy, "Fabrication and modeling of fused biconical tapered fiber couplers," Fiber Integr. Opt. **22**, 97–117 (2003).
[42]O. Parriaux, S. Gidon, and A. A. Kuznetsov, "Distributed coupling on polished single-mode optical fibers," Appl. Opt. **20**, 2420 (1981).
[43]M. Digonnet and H. Shaw, "Analysis of a tunable single mode optical fiber coupler," IEEE Trans. Microwave Theory Tech. **30**, 592–600 (1982).
[44]S. Takeda and A. Furusawa, "Universal quantum computing with measurement-induced continuous-variable gate sequence in a loop-based architecture," Phys. Rev. Lett. **119**, 120504 (2017).
[45]S. Takeda, K. Takase, and A. Furusawa, "On-demand photonic entanglement synthesizer," Sci. Adv. **5**, eaaw4530 (2019).
[46]A. Yariv and P. Yeh, *Photonics: Optical Electronics in Modern Communications*, 5th ed. (Oxford University Press, Oxford, 1996).